

# BIO-INSPIRED MICROBIAL CEMENTATION: ORGANIC ADDITIVES ENHANCING BIO-BASED CONSTRUCTION MATERIALS

Miao Liu<sup>1,2</sup>, Hanbin Luo<sup>1,2</sup>, Xu Chen<sup>1,2</sup>

*1 School of Civil and Hydraulic Engineering, Huazhong University of Science and Technology, Wuhan, China*

*2 National Center of Technology Innovation for Digital Construction, Huazhong University of Science and Technology, Wuhan, China*

## Abstract

Microbial cementation technology based on microbially induced calcium carbonate precipitation (MICP) is gaining increased attention as a sustainable construction solution. Although extracellular polymeric substances (EPS) are known to play a crucial role in the natural biocementation process, the strategic utilization of organic matrices to enhance MICP efficiency remains insufficiently explored. Inspired by biomineralization mechanisms, this study systematically investigated cost-effective and environmentally benign organic additives (including amino acid derivatives, animal/plant-derived macromolecules, and soluble polymers) for regulating mineralization processes. Significant variations in the mechanical and microstructural properties of biocements incorporating different additives were revealed through unconfined compressive strength test combined with material characterization techniques, including X-ray diffraction, thermogravimetric analysis, scanning electron microscopy, and X-ray photoelectron spectroscopy. Results demonstrated that the complexes formed through electrostatic interactions between calcium carbonate and polar functional groups in organic additives may be the primary mechanism underlying mechanical enhancement. Further analysis revealed that functional-group characteristics (type, density, and spatial configuration) synergistically interacted with the microenvironmental pH to control MICP mechanisms. Notably, polyacrylic acid, aspartic acid, and polyaspartic acid exhibited superior performance, enhancing the compressive strength of biocemented sandstone by more than 33% compared with that of the blank control group. This work established fundamental structure–function relationships for organic matrices in MICP, providing a rational design framework for developing bio-inspired construction materials with tailored properties.

**Keywords:** additive-mediated, biocementation, biomimetic, composite, effectiveness.

© 2025 The Authors. Published by the International Association for Automation and Robotics in Construction (IAARC) and Diamond Congress Ltd.

**Peer-review under responsibility of the scientific committee of the Creative Construction Conference 2025.**

## 1. Introduction

Biologically controlled mineralization processes, governed by organismal metabolism, yield composite materials with exceptional structural organization and mechanical performance. Representative biominerals—including nacre, bone, dental enamel, and avian eggshells—exhibit precisely assembled hierarchical architectures. Mechanistic studies reveal that the organic matrix-mediated mineralization process, even with minimal organic content (<5% [1]), plays a pivotal role in achieving superior mechanical properties through the formation of brick-and-mortar nanostructures [2]. Nevertheless, the inherently slow kinetics and limited scalability of natural biomineralization pose challenges for their direct application in large-scale construction projects.

Historical precedents of biologically inspired construction materials can be traced to mid-11th century China during the Northern Song Dynasty, where cultured oysters were strategically used to reinforce bridge foundations in the iconic Luoyang Bridge (Wan'an Bridge). This early innovation foreshadowed contemporary advancements, as exemplified by Tiano et al.'s [3] breakthrough in biomimetic calcium carbonate synthesis using organic matrices extracted from mollusk shells for stone conservation. These

*Corresponding author email address: liumiaohust@gmail.com*

milestones have catalysed ongoing research into microbial-mediated cementitious materials and bio-inspired construction technologies.

The urease-catalysed microbial-induced calcium carbonate precipitation (MICP) mechanism operates through two sequential reactions: ureolytic bacteria hydrolyse urea (Eq. 1) to generate carbonate ions, which subsequently combine with calcium cations from external sources to precipitate  $\text{CaCO}_3$  (Eq. 2).



As foundational decomposers, ureolytic bacteria inherently prioritize urea hydrolysis for metabolic energy generation over material synthesis, leading to suboptimal MICP regulation and mineral composites lacking organic matrices. Evidently, the mechanical performance of such biocemented sandstone strongly depends on the chemical characteristics of supplemented organic additives. To circumvent this biological constraint, researchers have adopted a biomimetic compensation strategy through exogenous organic additives—including low-molecular-weight compounds [4], synthetic polycarboxylic acids, and biopolymers (plant/animal-derived polysaccharides [5-7]) and proteins [8]). These interventions partially replicate the organic matrix functionalities, with additive-induced calcium precipitation efficiency reaching 96.07%[7]. Despite these technological adaptations, critical knowledge gaps persist between biomineralization theory and engineering practice. The structure-function relationships governing organic additive efficacy in biocemented sandstone remain poorly characterized, forcing material selection to rely on empirical trial-and-error approaches rather than mechanistic design principles. This persistent knowledge gap in organic matrix selection strategies significantly hinders the practical implementation of biogenic construction or bio-inspired construction technologies. This study aimed to bridge the gap between biomineralization theory and applied microbial cementation techniques through systematic experimental analysis.

In the present study, we used multi-scale analytical techniques to characterize sandstone specimens treated with organic-augmented MICP. These techniques include unconfined compressive strength (UCS) testing, X-ray diffraction (XRD), thermogravimetric analysis (TGA), scanning electron microscopy (SEM), and X-ray photoelectron spectroscopy (XPS). Comparative assessment of organic-inorganic composite compatibility was performed through microstructure-property correlations. Finally, we evaluated the engineering implications of our findings for sustainable construction materials.

## 2. Materials and methodology

### 2.1. Raw Materials

The ureolytic bacterium *Sporosarcina pasteurii* (BNCC 337394) was acquired from the BeNa Culture Collection (Beijing, China). Bacteria were cultured under aerobic conditions at 30 °C until reaching the target optical density of ~1.8.

Medium-grained quartz sand (particle size: 0.63–1.25 mm) was sieved prior to use, with detailed physical properties reported in our prior investigations [9], [10]. All organic additives (Table 1) were procured from Aladdin Biochemical Technology Co., Ltd. (Shanghai, China) with ≥98% purity. Experimental groups supplemented with organic additives were compared against an additive-free blank control (denoted as BC) prepared using sterile deionized water as substitute.

Table 1. Basic properties of selected organic additives.

No.	Additives	Typical functional groups or side chains	pH Adjustment
Asp_pH3	L-Aspartate	–COOH, –NH <sub>2</sub>	pH 3
Asp_pH4	L-Aspartate	–COOH, –NH <sub>2</sub>	pH 4
Asp_pH6	L-Aspartate	–COOH, –NH <sub>2</sub>	pH 6
PASP	Polyaspartic acid	–COOH	pH 7
PAA	Polyacrylic acid	–COOH	pH 7

AA	Alginic acid	–OH (major), –COOH	pH 7
SA	Sodium alginate	–OH (major), –COOH/–COONa	pH 7
CACS	Carboxylated chitosan	–OH (major), –COOH, –NH <sub>2</sub>	pH 7
XG	Xanthan gum	–OH (major), –COOH, Pyruvate group	pH 7
WG	Welan gum	–OH (major), –COOH, Pyruvate group	pH 7

## 2.2. Experimental design and preparation

Eleven experimental groups were established using cylindrical PVC molds (inner diameter = 39.1 mm, height = 130 mm), with each group comprising three specimens for mechanical characterization and one reserve specimen for material analysis. Prior to assembly, Interior surfaces of each mold were lined with vaseline-coated polyethylene sheets to facilitate demolding. Each mold received 144 g of medium-grained quartz sand, which was compacted through vibrational densification to achieve an 80 mm sand column height (bulk density = 1.50 g/cm<sup>3</sup>). Permeable stones were positioned at the top and bottom of the sand column. Specimens were saturated with deionized water via upward percolation at 5 mL/min prior to MICP treatment.

The cementation solution comprised 0.6 M urea, 0.6 M CaCl<sub>2</sub>, and organic additives (Table 1), with concentrations set at 0.2 M for small-molecule additives and 3 g/L for polymeric compounds. Xanthan gum-containing solutions were mechanically mixed for 30 min at 500 rpm, whereas other polymer solutions required 6 h mixing. Bacterial suspension (volume equivalent to initial pore volume of the sandstone) was gravity fed through the upper injection port at 5 mL/min, followed by 3 h standing to enable microbial attachment. Subsequently, an equivalent-volume cementation solution was introduced by gravity-driven flow at 5 mL/min through the upper injection port. The cementation solution and bacterial solution were supplemented every 12 and 72 h, respectively. Post-treatment specimens were rinsed with two pore volumes of deionized water and oven dried at 40 °C (72 h). Finally, the samples were subjected to mechanical testing and microscopic analysis to evaluate the effect of biocementation.

## 2.3. Characterization methods

The unconfined compressive strength was measured using a triaxial apparatus at 1.0 mm/min loading rate. This preliminary study assessed additive efficacy rather than optimizing concentrations. The polymorphs of precipitates were identified by X-ray powder diffractometer (X'Pert3 powder, PANalytical B.V., Netherlands) that is operated under a CuK $\alpha$  radiation ( $\lambda = 1.54 \text{ \AA}$ ). The samples were scanned at 4°/min ranging from 5 to 70°(2 $\theta$ ). Polymorph ratios of CaCO<sub>3</sub> were quantified via relative intensity method [11]. Thermal stability of the precipitate was evaluated by TG (STA300, Hitachi High-Tech, Japan) under a nitrogen flow. The samples were heated from 30 to 1000 °C temperature range at a heating rate of 10 °C/min. The microstructural characterization of the specimens used field-emission SEM (GeminiSEM300, Carl Zeiss, Germany) and XPS (AXIS-ULTRA DLD-600W, Shimadzu-Kratos, Japan) in the range of 2000–400 eV. In instances where XPS peaks exhibited multiple components, a peak-fitting program was adopted by assuming a 100% Gaussian peak shape.

## 3. Results and discussion

### 3.1. Compressive strength

Biocementation efficacy of various organic additives is shown in Fig. 1. Notably, Asp\_6, PASP, PAA, CACS, and WG enhance compressive strength of biocemented sandstone by 64.5%, 33.0%, 94.4%, 29.6%, and 25.7%, respectively. Considering the functional group type of the additive, both carboxyl-containing small molecules and polymers rich in carboxylic acid side chains have good mechanical enhancement effects on biocementation. This enhancement was correlated with their abundant negatively charged groups (–COOH/–OH) that chelated Ca<sup>2+</sup> and formed complexes with biomineralization products. Polymeric additives (PAA/PASP) demonstrated superior performance, attributed to their high-density –COOH groups and extended carbon chains that stabilized mineralization frameworks. Notably, some specific proteins rich in aspartic acid are usually used by living organisms as indispensable matrix proteins in the formation of natural biomineralization products, which may mirror the wisdom of nature. Hydroxyl-rich additives (CACS/WG) exhibited moderate enhancement, suggesting that electrostatic potential governed mineral–organic interactions. Functional-group

speciation and electrochemical compatibility emerged as critical design parameters for bio-inspired cementation.

From the perspective of the pH of the applied additives, Asp cannot play a positive role under acidic conditions. acidic conditions (Asp\_3/Asp\_4 groups) may compromise biocementation through dual mechanisms: (1) microbial inactivation and (2) carbonate dissolution. Consequently, the compressive strength of the Asp\_3 and Asp\_4 groups was low.

Unexpectedly, the compressive strength of SA-incorporated biocemented sand was only 61.5% of that of AA, which means that SA underperformed compared with AA despite the former's superior  $\text{Ca}^{2+}$  affinity. Three reasons have been proposed by mechanism analysis:

- Although SA contributed to the formation of pre-organized "carboxylate-calcium ion" mineralization precursor, the viscosity caused by rapidly forming ion cross-linked gel networks may impede ion diffusion and lead to less structured biomineralised materials.
- Gel shrinkage may generate internal stresses and interfacial defects.
- AA's partial protonation enabled balanced chelation–diffusion dynamics, promoting uniform crystal growth. Additionally, the abundant un-ionized carboxyl groups of AA also had the function of chelating Ca ions.

Compared with the BC group, AA and SA did not play a positive role. It proved that dosage optimization was critical, that is, excessive additives (AA/SA groups) disrupted mineral cohesion, highlighting non-monotonic structure–property relationships.

The application method of organic additives may have a significant impact on the biocementation. As a natural bacterial polysaccharide, XG can reportedly enhance biocementation. This study observed that XG cannot enhance biocementation owing to insufficient dispersion time (30 min), which was insufficient for complete macromolecular unfolding. Conversely, WG—a polysaccharide structurally analogous to XG—achieved full dispersion and demonstrated effective biocementation enhancement.

The above analysis may not be perfect, so further microscopic characterization will be carried out below.

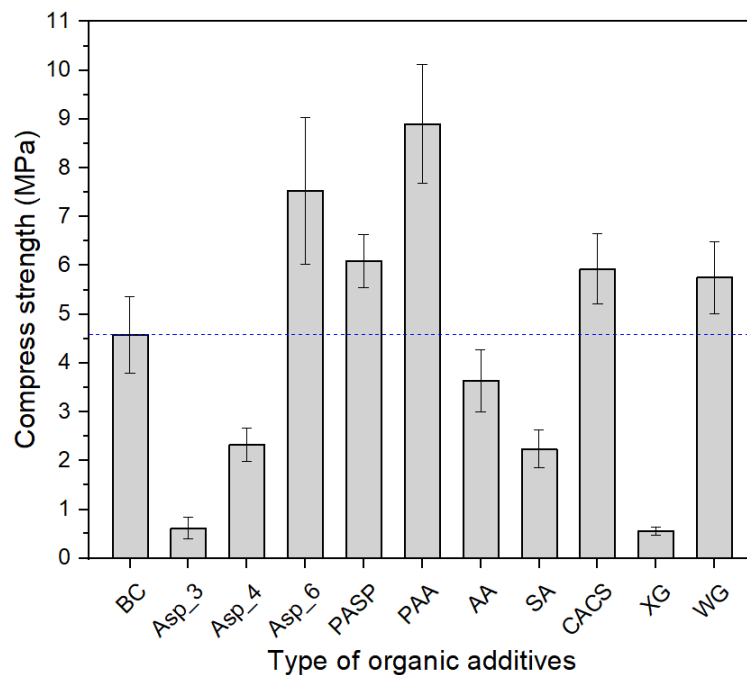


Fig. 1. Compressive strength of biocemented sandstone mediated by various organic additives.

### 3.2. Mineral analysis

To address the unresolved mechanistic question of how organic additives regulate Biogenic  $\text{CaCO}_3$  crystallization, XRD analysis can be employed to elucidate their coordination interactions with

crystallographic planes through systematic characterization of peak intensity variations in calcite or vaterite polymorphs. Fig. 2 demonstrates the crystallographic modulation of biogenic  $\text{CaCO}_3$  by organic additives. The thermodynamic phase transformation from vaterite to calcite spontaneously occurred. Organic matter (e.g., Asp, PASP, PAA, and CACS) with strong negatively charged functional groups promoted vaterite stabilization. This vaterite stabilization was correlated with enhanced mechanical performance (compressive strength in Fig. 1), suggesting a charge-mediated crystallization mechanism wherein carboxylate-rich matrices chelated nascent  $\text{CaCO}_3$  to form an organic–inorganic hybrid structure through electrostatic interactions. This phenomenon kinetically arrested the thermodynamically favored calcite formation. The robust bonding between the organic matrix and inorganic minerals is manifested macroscopically as an enhancement in cementation levels, while at the microscopic scale, it corresponds to the stabilization of metastable crystal phases (e.g., vaterite) by organic components. This mechanism provides valuable insights for the strategic selection of organic matrices in future applications.

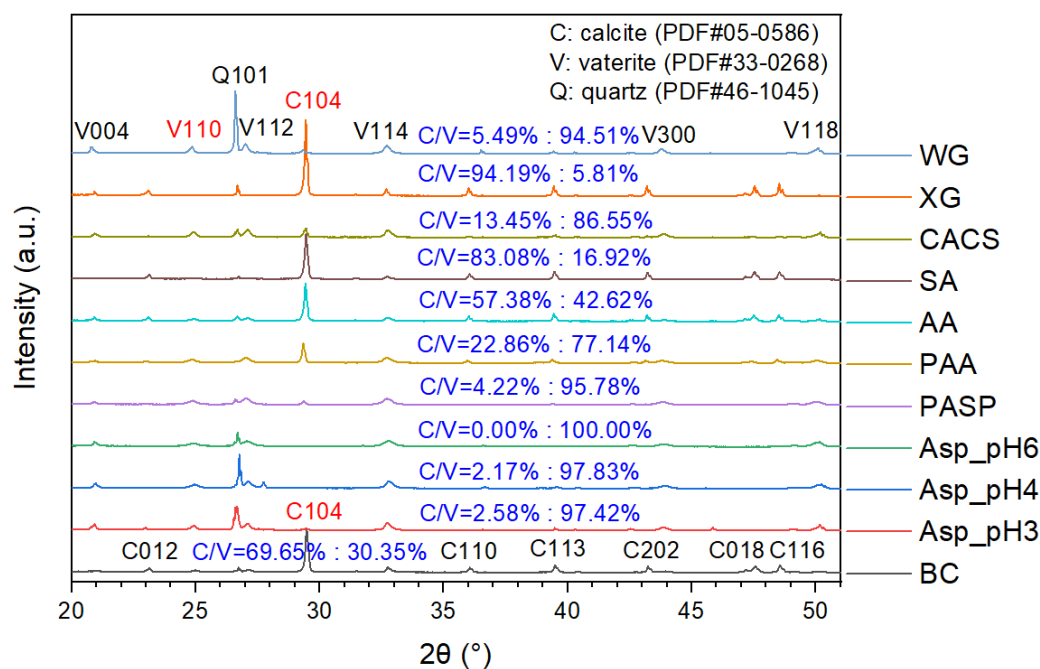


Fig. 2. XRD patterns of MICP products incorporating various organic additives.

### 3.3. Thermogravimetric analysis

The TG curves of organic-mediated biocement are presented in Fig. 3, with key mass-loss data at 160 °C, 550 °C, 750 °C, and 920 °C, as summarized in Table 2. Four distinct decomposition stages were identified: (1) dehydration (<160 °C), (2) pyrolysis of organic matter and residual dehydration (160–550 °C), (3)  $\text{CaCO}_3$  decomposition (550–750 °C), and (4) carbonization of organic components (750–920 °C). An organic-to-inorganic ratio  $(T3-T4)/(T2-T3)$  was formulated to quantify the organic matrix content in the organic matrix–inorganic mineral composite.

All additives' organic fractions increased compared with those of the blank control (BC), with small-molecule Asp exhibiting the highest organic retention (Table 2). Furthermore, the limited functional groups of small molecules necessitated elevated additive concentrations, a practice often overlooking cost inefficiency in prior studies [12]. Although organic–inorganic compatibility mediated mechanical enhancement through interfacial bonding, no convincing monotonic correlation existed between organic content and compressive strength. Notably:

- XG-treated specimens may display compromised strength owing to water retaining hydrogel-induced structural defects. In other words, the excessive water-absorption capacity of organic additives may weaken the bonding power of biocement.
- AA-modified specimens showed reduced cohesion despite moderate organic content.

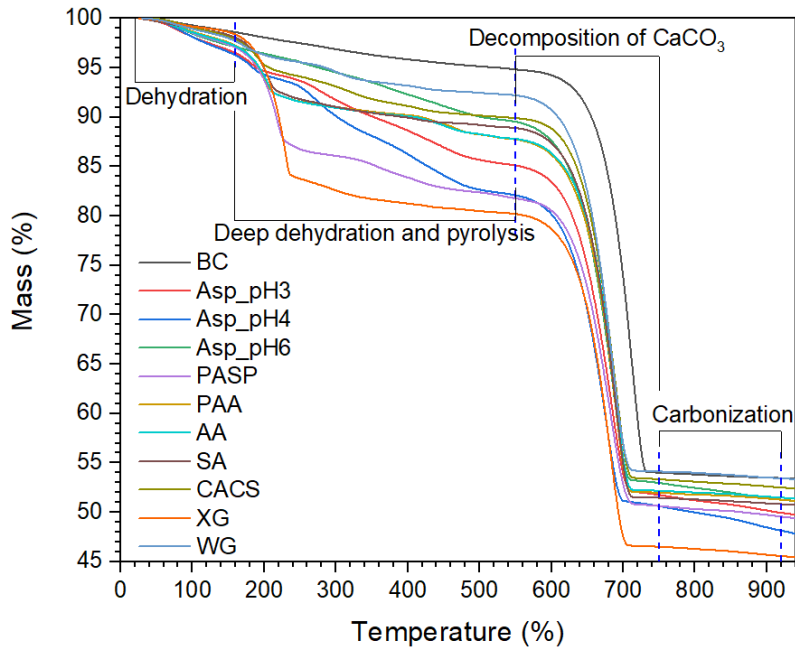


Fig. 3. TG curves of biocement mediated by various organic additives.

Table 2. Main TG data of bio-based carbonate cement with various organic additives.

No.	T1(160°C)	T2(550°C)	T3(750°C)	T4(920°C)	T2–T3	T3–T4	(T3–T4)/(T2–T3)
BC	98.60	94.83	54.00	53.46	40.82	0.54	1.33%
Asp_pH3	96.48	85.11	51.76	49.95	33.34	1.81	5.44%
Asp_pH4	96.26	82.10	50.63	48.14	31.48	2.48	7.89%
Asp_pH6	97.10	89.53	52.97	51.28	36.56	1.69	4.62%
PASP	97.04	81.78	50.63	49.57	31.14	1.07	3.42%
PAA	97.23	87.74	51.97	51.27	35.77	0.70	1.96%
AA	97.18	87.79	52.17	51.49	35.62	0.69	1.93%
SA	98.05	88.90	51.46	50.83	37.43	0.63	1.69%
CACS	97.83	89.90	53.34	52.51	36.56	0.83	2.27%
XG	98.35	80.20	46.51	45.57	33.69	0.94	2.80%
WG	97.68	92.21	54.12	53.43	38.09	0.69	1.82%

### 3.4. Microstructure analysis

To further investigate the microstructural regulation of biocementation by organic additives, Fig. 4 displays the morphology of MICP products mediated by these additives. In the additive-free control (Fig. 4a), four-cycle biogrouting generated a core–shell structure in biocement, where aged calcite exhibited densification and peripheral regions showed minor unstable vaterite fractions undergoing delayed phase transformation.

pH-dependent bacterial viability was observed. In particular, acidic conditions (pH 4, Fig. 4b) induced cell lysis, whereas near-neutral environments (pH 6, Fig. 4c) preserved cellular integrity. The crystal form was vaterite under the regulation of Asp (Fig. 4(b)(c)). PAA-regulated mineralization yielded the densest vaterite (Fig. 4d), whereas AA facilitated localized oriented calcite growth with regular morphologies (Fig. 4e). SA-incorporated systems (Fig. 4f) exhibited a higher rhombohedral calcite fraction than AA-modified counterparts (Fig. 4e), with SA facilitating intercrystalline bridging. XG induced calcite cross-linking (Fig. 4g), contrasting with WG organic–inorganic fusion (Fig. 4h).

This polymorph distribution consistency between SEM observations (Fig. 4) and XRD analyses (Fig. 2) validated additive-specific crystallization pathways.

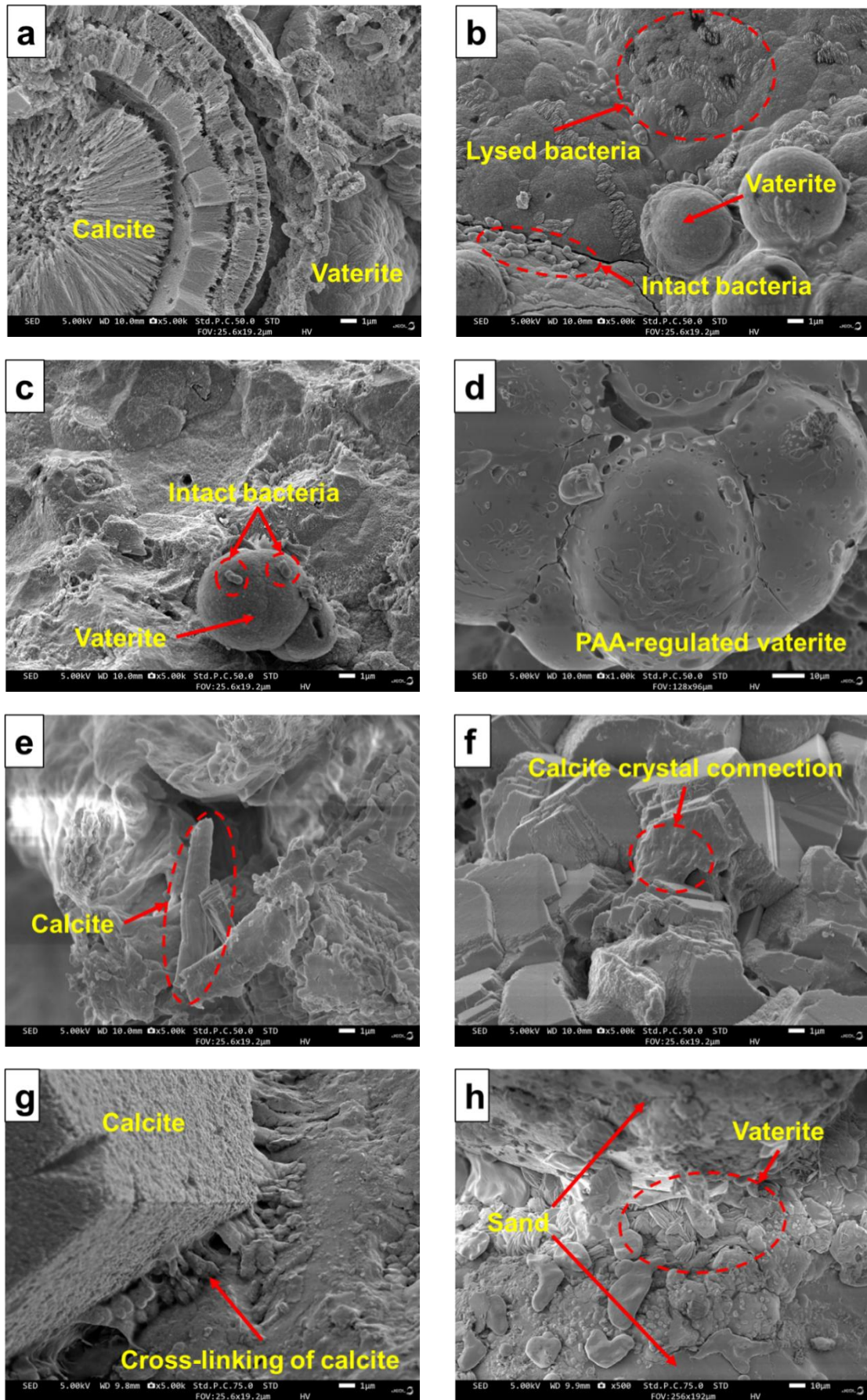


Fig. 4. SEM images of biocement incorporating different organic additives: (a) BC, (b) Asp\_4, (c) Asp\_6, (d) PAA, (e) AA, (f) SA, (g) XG, and (h) WG.

### 3.5. Regulation mechanism of organic additives on biomineralization

XPS analysis offers direct evidence of interfacial bonding interactions between the organic matrices and inorganic minerals. As shown in Fig. 5, the Ca 2p spectra of both the BC and PASP-modified groups exhibit distinct chemical shifts, with quantitative peak data provided in Table 3. The spectral features included: (1) peak2 (~351.0 eV) and peak3 (~347.5 eV), corresponding with Ca 2p<sub>1/2</sub> and 2p<sub>3/2</sub> orbitals; and (2) peak1 (~355.0 eV), attributed to Ca<sup>2+</sup> coordination with electron-withdrawing groups (–COOH, –OH, etc.) in organic matrices, which reduced electron cloud and increased binding energy

In the BC group (Fig. 5a), without additives, the insufficient intrinsic bacterial organic matter restricted the interfacial interactions with CaCO<sub>3</sub> during MICP. Table 3 reveals that most of the organic additives significantly enhanced peak1 intensity, with high-performance additives (Asp, PASP (Fig. 5b), PAA, CACS, and WG) showing the strongest peak1 signals. This charge redistribution preliminarily revealed the mechanical-enhancement mechanism of hybrid composites through interfacial electron coupling.

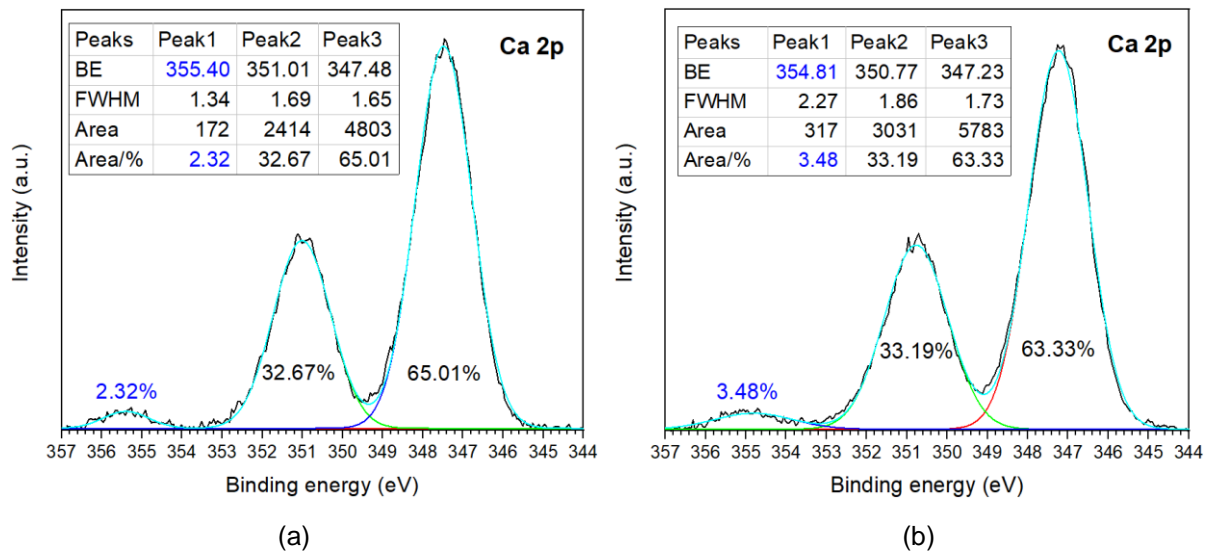


Fig. 5. XPS analysis of biocement with organic additives: (a) Ca 2p spectrum of BC group, and (b) Ca 2p spectrum of PASP-modified group.

Table 3. XPS spectral parameters of Ca 2p peaks in MICP composites.

No.	Peak1		Peak2		Peak3	
	BE (eV)	Area (%)	BE (eV)	Area (%)	BE (eV)	Area (%)
BC	355.40	2.32	351.01	32.67	347.48	65.01
Asp_pH3	355.14	2.38	351.22	32.18	347.69	65.44
Asp_pH4	354.93	2.80	350.84	32.44	347.32	64.76
Asp_pH6	354.77	4.83	350.71	32.48	347.19	62.68
PASP	354.81	3.48	350.77	33.19	347.23	63.33
PAA	355.20	4.74	351.16	32.32	347.62	62.93
AA	355.12	3.03	350.92	32.63	347.39	64.34
SA	355.28	2.14	351.06	32.63	347.54	65.23
CACS	355.18	3.57	350.82	32.16	347.29	64.26
XG	355.35	3.65	351.09	32.36	347.57	63.99
WG	355.09	6.91	350.92	31.75	347.37	61.34

## 4. Conclusion

This study investigated MICP-based biocementation products mediated by different types of organic additives through multi-scale characterization and established preliminary structure–property relationships in bio-inspired construction materials. Three principal conclusions emerged:

(1) The binding force between the negatively charged functional groups of organic additives and calcium carbonate was a key factor in enhancing biocementation efficiency.

(2) The pH conditions during organic additive application and their dispersion state in the liquid phase influenced biocementation outcomes.

(3) The organic additives PAA, Asp, and PASP can improve the mechanical performance of traditional carbonate biocement by more than 33%.

This study elucidates preliminary correlations between the mechanical properties and microscopic physicochemical characteristics of bio-inspired carbonate mortar, a material system emblematic of the transformative paradigm shift toward biogenic construction in modern engineering. However, the dosage and application methods of organic additives require further optimization. Future research will prioritize the molecular-scale design of organic matrices to develop advanced bio-based construction materials with biomimetic functionalities.

### Acknowledgements

This work was supported by the National Natural Science Foundation of China (Grant No. U21A20151).

### References

- [1] F. Song, A. K. Soh, and Y. L. Bai, "Structural and mechanical properties of the organic matrix layers of nacre," *Biomaterials*, vol. 24, no. 20, pp. 3623–3631, Sep. 2003, doi: 10.1016/S0142-9612(03)00215-1.
- [2] Z. Tang, N. A. Kotov, S. Magonov, and B. Ozturk, "Nanostructured artificial nacre," *Nat. Mater.*, vol. 2, no. 6, pp. 413–418, Jun. 2003, doi: 10.1038/nmat906.
- [3] P. Tiano, "Stone reinforcement by calcite crystal precipitation induced by organic matrix macromolecules," *Stud. Conserv.*, vol. 40, no. 3, pp. 171–176, Aug. 1995, doi: 10.1179/sic.1995.40.3.171.
- [4] M. Chen, D. Cao, B. Li, H. Pang, and C. Zheng, "Sodium citrate increases the aggregation capacity of calcium ions during microbial mineralization to accelerate the formation of calcium carbonate," *Environ. Res.*, vol. 224, p. 115479, May 2023, doi: 10.1016/j.envres.2023.115479.
- [5] F. Manoli, S. Koutsopoulos, and E. Dalas, "Crystallization of calcite on chitin," *J. Cryst. Growth*, vol. 182, no. 1–2, pp. 116–124, Dec. 1997, doi: 10.1016/S0022-0248(97)00318-7.
- [6] T. H. K. Nawarathna, K. Nakashima, and S. Kawasaki, "Chitosan enhances calcium carbonate precipitation and solidification mediated by bacteria," *Int. J. Biol. Macromol.*, vol. 133, pp. 867–874, Jul. 2019, doi: 10.1016/j.ijbiomac.2019.04.172.
- [7] Z. Wang et al., "Chitosan and carboxymethyl chitosan mimic biomineralization and promote microbially induced calcium precipitation," *Carbohydr. Polym.*, vol. 287, p. 119335, Jul. 2022, doi: 10.1016/j.carbpol.2022.119335.
- [8] Z. Zhang, K. Tong, L. Hu, Q. Yu, and L. Wu, "Experimental study on solidification of tailings by MICP under the regulation of organic matrix," *Constr. Build. Mater.*, vol. 265, p. 120303, Dec. 2020, doi: 10.1016/j.conbuildmat.2020.120303.
- [9] M. Liu, L. Cai, and H. Luo, "Effect of nano-silica on microbiologically induced calcium carbonate precipitation," *Constr. Build. Mater.*, vol. 314, p. 125661, Jan. 2022, doi: 10.1016/j.conbuildmat.2021.125661.
- [10] M. Liu, X. Chen, L. Cai, and H. Luo, "Regulatory mechanism of humic substances on microbially induced carbonate precipitation," *Constr. Build. Mater.*, vol. 458, p. 139581, Jan. 2025, doi: 10.1016/j.conbuildmat.2024.139581.
- [11] C. G. Kontoyannis and N. V. Vagenas, "Calcium carbonate phase analysis using XRD and FT-Raman spectroscopy," *The Analyst*, vol. 125, no. 2, pp. 251–255, 2000, doi: 10.1039/a908609i.
- [12] Y. Diao et al., "Development and optimization of biomimetic-chemically induced carbonate precipitation: A review of recent research," *Biogeotechnics*, vol. 3, no. 1, p. 100110, Mar. 2025, doi: 10.1016/j.bgtech.2024.100110.